Inorganic Chemistry

ARTICLE

pubs.acs.org/IC

# Synthesis, Crystal and Electronic Structures, and Properties of the New Pnictide Semiconductors $A_2CdPn_2$ ($A$ = Ca, Sr, Ba, Eu; $Pn$ = P, As)

Jian Wang, Min Yang, Ming-Yan Pan, Sheng-Qing Xia,* and Xu-Tang Tao

State Key Laboratory of Crystal Materials, Institute of Crystal Materials, Shandong University, Jinan, Shandong 250100, People's Republic of China

Hua He, Gregory Darone, and Svilen Bobev*

Department of Chemistry and Biochemistry, University of Delaware, Newark, Delaware 19716, United States

Supporting Information

**ABSTRACT:**

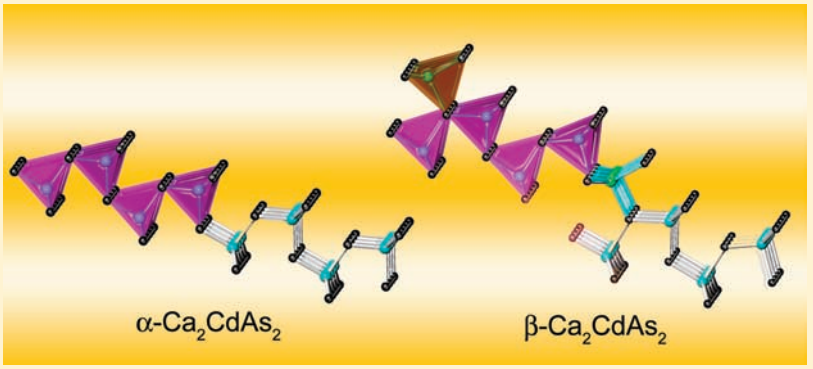


A series of ternary Zintl phases, $Ca_2CdP_2$, $Ca_2CdAs_2$, $Sr_2CdAs_2$, $Ba_2CdAs_2$, and $Eu_2CdAs_2$, have been synthesized through high temperature metal flux reactions, and their structures have been characterized by single-crystal X-ray diffraction. They belong to the $Yb_2CdSb_2$ structure type and crystallize in the orthorhombic space group $Cmc2_1$ (No. 36, $Z$ = 4) with cell dimensions of $a$ = 4.2066(5), 4.3163(5), 4.4459(7), 4.5922(5), 4.4418(9) Å; $b$ = 16.120(2), 16.5063(19), 16.904(3), 17.4047(18), 16.847(4) Å; $c$ = 7.0639(9), 7.1418(8), 7.5885(11), 8.0526(8), 7.4985(16) Å for $Ca_2CdP_2$ (R1 = 0.0152, wR2 = 0.0278), $Ca_2CdAs_2$ (R1 = 0.0165, wR2 = 0.0290), $Sr_2CdAs_2$ (R1 = 0.0238, wR2 = 0.0404), $Ba_2CdAs_2$ (R1 = 0.0184, wR2 = 0.0361), and $Eu_2CdAs_2$ (R1 = 0.0203, wR2 = 0.0404), respectively. Among these, $Ca_2CdAs_2$ was found to form with another closely related structure, depending on the experimental conditions—monoclinic space group $Cm$ (No. 8, $Z$ = 10) with lattice constants $a$ = 21.5152(3) Å, $b$ = 4.30050(10) Å, $c$ = 14.3761(2) Å and $\beta$ = 110.0170(10)° (R1 = 0.0461, wR2 = 0.0747). UV/vis optical absorption spectra for both forms of $Ca_2CdAs_2$ show band gaps on the order of 1.0 eV, suggesting semiconducting properties, which have also been confirmed through electronic band structure calculations based on the density-functional theory. Results from differential scanning calorimetry measurements probing the thermal stability and phase transitions in the two $Ca_2CdAs_2$ polymorphs are discussed. Magnetic susceptibility measurements for $Eu_2CdAs_2$, indicating divalent $Eu^{2+}$ cations, are presented as well.

## INTRODUCTION

The classical Zintl phases are compounds of the alkali or alkaline-earth metals and the post-transition elements from group 13−15. They are usually considered as electron-precise compounds, that is, semiconductors or even insulators, following the assumption that a complete electron transfer from the cations to the anions occurs.[1−3] However, there are many examples of metallic behavior, particularly in systems with heavy $p$-elements like In, Tl, Sn, Sb, or Bi, which apparently lack the band gap often seen with the light group-congeners.[4,5] In the past two decades, the Zintl concept has been extended to include some of the transition metals and/or several members of the lanthanide series.[6] Our groups have contributed to this field by exploring the $A$-$T$-$Pn$ ternary systems (where $A$ = divalent alkaline-earth or rare-earth metals; $T$ = Mn, Zn, Cd; and $Pn$ = pnictogen elements), and we have already reported numerous new ternary phases with diverse structures among these elements.[7,8] Other research groups have studied the complexity of these compounds in conjunction with their physical properties and have identified colossal magnetoresistance,[9] interesting ferromagnetism and antiferromagnetism,[10] mixed-valency,[11] and so forth, within the realm of the same systems.

**Received:** February 14, 2011
**Published:** July 25, 2011

Very recently, several antimonide examples have attracted new attention for their potential thermoelectric applications.[12,13]

Despite all fundamental and practical research on Zintl phases, there appears to be a lack of reports on the feasibility of such materials for nonlinear optical (NLO) applications.[14] On the basis of the definitions above, one could reason that Zintl phases could be suitable in the mid- and far-IR regions, in analogy with some well-known $ABC_2$ chalcopyrite semiconductors, such as $ZnGeP_2$,[15] and $AgGaS_2$,[16] which are commercially available, although their high-power applications are limited because of their low laser damage thresholds. To mitigate this problem, new IR NLO materials are currently being developed worldwide.[17−20] In this regard, the recently discovered Zintl phases $A_2CdSb_2$ ($A$ = Ca, Yb with Sr, Ba, Eu as dopants),[8] have piqued our interest because of the noncentrosymmetric structural arrangement and the presence of a band gap in their electronic structure. With a consideration of ensuring a wider gap, better suited for the IR region, we embarked on studying the arsenide and phosphide members of this system.

In this paper, we report the new ternary Zintl phases, $Ca_2CdP_2$, $Ca_2CdAs_2$, $Sr_2CdAs_2$, $Ba_2CdAs_2$, and $Eu_2CdAs_2$, crystallizing in the orthorhombic $Yb_2CdSb_2$ structure type. $Ca_2CdAs_2$ is polymorphic, with the second form belonging to a new structure type with the monoclinic space group $Cm$. Both structures are noncentrosymmetric and feature polyanionic layers, based on corner-shared $CdP_4$ or $CdAs_4$ tetrahedra. Thermal analyses on the two polymorphs indicate that the monoclinic phase, hereafter referred to as $\beta$-$Ca_2CdAs_2$, is favored at higher temperature over the orthorhombic phase ($\alpha$-$Ca_2CdAs_2$). The semiconducting properties of these new compounds were characterized as well, which were supported by computation results.

## EXPERIMENTAL SECTION

**Synthesis.** All starting materials were handled inside an argon-filled glovebox or under vacuum to avoid possible oxidation or contamination from air. The elements were commercial grade and used as received: Ca (Alfa, shot, 99.5% metals basis), Sr (Alfa, granules, 99% metals basis), Ba (Alfa, rod, 99+% metals basis), Eu (Alfa, rod, 99.9% metals basis), Cd (Alfa, shot, 99.999%), P (Alfa, lump, 99.999%), As (Alfa, lump, 99.999%). The crystals of the title compounds were obtained by utilizing molten Cd, Sn (Alfa, granules, 99.9%), or Pb (Alfa, shot, 99.9%), as the metal fluxes.

**$Sr_2CdAs_2$, $Ba_2CdAs_2$ and $Eu_2CdAs_2$.** Crystals of all three compounds were grown by either using Cd or Pb as metal fluxes, and the synthesis procedures were as follows: (1) $A$ ($A$ = Sr, Ba, or Eu), Cd and As were loaded in alumina crucibles in a molar ratio of $A$/Cd/As = 1:50:1. Utilizing a large excess of cadmium in such reactions was found necessary for obtaining high quality single-crystals, which is possibly due to the low boiling point of Cd and/or the poor solubility of the products in the Cd flux. The crucibles were subsequently sealed in evacuated fused silica jackets. The reaction mixtures were heated to 700 °C at a rate of 200 °C/h and homogenized at this temperature for 24 h, followed by a slow cooling to 400 °C at a rate of 3 °C/h and then the excess molten Cd was decanted immediately. 2) $A$ ($A$ = Sr, Ba or Eu); Cd and As were loaded in a molar ratio of $A$/Cd/As = 2:1:2. In this case, a modified procedure using 15-fold excess of lead as the flux was applied, which proved to be sufficient in growing good single crystals. The synthetic procedure was the same as before, except that the mixtures of elements were heated to 960 °C at a rate of 60 °C/h and homogenized at this temperature for 20 h, followed by cooling to 500 °C at a rate of 30 °C/h. At this point the excess molten Pb was removed. The products of these compounds were black, needle-shaped crystals, which appeared sensitive to air except for $Eu_2CdAs_2$. The latter was stable in dry air outside the glovebox for several days.

**$Ca_2CdP_2$.** Utilizing Sn as the metal flux was determined to be the best synthetic route to $Ca_2CdP_2$ (probably because of the good solubility of P in Sn). The reaction was carried out with the molar ratio of Ca/Cd/P/Sn = 2:1:2:30, by following the same heat treatments, as described for $A_2CdAs_2$ ($A$ = Sr, Ba, Eu). The typical products of the reactions in Sn flux were small shiny red pieces for $Ca_2CdP_2$ and some irregular silver pieces of Sn−P binaries. The crystals of $Ca_2CdP_2$ were determined to be stable in air for a couple of weeks.

**$Ca_2CdAs_2$.** Reactions in the Ca−Cd−As system proved the most difficult to sort out. Various experiments aimed at producing $Ca_2CdAs_2$, which is isostructural with the corresponding phosphide and $A_2CdAs_2$ ($A$ = Sr, Ba, Eu) led to the identification of the monoclinic $\beta$-$Ca_2CdAs_2$ phase. The best crystals of this compound were grown from Cd flux, but at a higher homogenization temperature (900 °C). The orthorhombic $\alpha$-$Ca_2CdAs_2$ phase was only obtained from Sn flux by applying the same procedure as that for $Ca_2CdP_2$. Both crystals were black, lustrous with needle-like morphology and their shiny appearance was preserved for a couple of weeks when exposed in air.

The existence of two $Ca_2CdAs_2$ polymorphs prompted us to further explore the phase relationship in this system. Extensive efforts to alter the temperature profiles, however, did not lead to conclusive results. For example, $\alpha$-$Ca_2CdAs_2$ phase could be made in Sn-flux at temperatures ranging from 700 to 900 °C, while the monoclinic $\beta$-$Ca_2CdAs_2$ phase formed only from Cd flux at 900 °C; Cd-flux reactions at 700 °C did not produce crystalline products. This may suggest that: 1) inclusions from the flux are crucial for the formation of $\alpha$-$Ca_2CdAs_2$ phase, although this is highly unlikely given that all other $A_2CdAs_2$ ($A$ = Sr, Ba, Eu) compounds with the same structure can be synthesized from Cd, Sn or Pb fluxes (as discussed previously for $A_2CdSb_2$ ($A$ = Ca, Yb)[8a]); 2) the nucleation and crystal growth of the two $Ca_2CdAs_2$ polymorphs are affected in different ways in Cd or Sn "solvent". This conclusion is supported by the results from thermal analysis, which shows that both forms are incongruent melting phases and cannot be converted from one form to another.

$Yb_2CdAs_2$, neither with the orthorhombic structure of the $\alpha$-phase nor with the monoclinic structure of $\beta$-$Ca_2CdAs_2$, could not be synthesized under the above-discussed conditions. $A_2CdAs_2$ ($A$ = Sr, Ba, Eu), isostructural to the $\beta$-$Ca_2CdAs_2$ phase could not be identified either.

***Caution!*** *Cd and As are highly toxic and experiments related to these elements must be handled with extreme care! The high vapor pressure of cadmium at the reaction temperature of 900 °C may cause the sealed silica tubes to break, which could lead to potentially hazardous conditions. Use of well-sealed and thick (1.5+ mm) silica tubes is necessary to reduce such risks.*

**Single Crystal X-ray Diffraction and Structure Determination.** Crystals suitable for data collection were selected in a glovebox and cut in Paratone N oil to desired dimensions. The data collections were performed on a Bruker SMART APEX-II CCD area detector on a D8 goniometer using graphite-monochromated Mo−Kα radiation ($\lambda$ = 0.71073 Å) with the $\omega$ scan method. The crystals prone to decomposition in air were handled with care, and the corresponding data collections were completed under inert atmosphere, achieved by using a nitrogen gas stream. Preliminary lattice parameters and orientation matrices were obtained from three sets of frames. Data reduction and integration, together with global unit cell refinements were done by the INTEGRATE program of the APEX2 software.[21] Semiempirical absorption corrections were applied using the SCALE program for area detector.[21] The structures were solved by direct methods and refined by full matrix least-squares methods on $F^2$ using SHELX.[22] In the last refinement cycles, the atomic positions for $\beta$-$Ca_2CdAs_2$ (new structure type, Pearson symbol $mC50$) were standardized using the program Structure TIDY;[23] for $\alpha$-$Ca_2CdAs_2$ and the other structures ($Yb_2CdSb_2$ structure type, Pearson symbol $oC20$), the atomic coordinates were taken from the literature.[8a] All structures were refined to convergence with anisotropic displacement parameters.


dx.doi.org/10.1021/ic200286t |Inorg. Chem. 2011, 50, 8020–8027

**Table 1. Selected Crystal Data and Structure Refinement Parameters for α-$Ca_2CdAs_2$, β-$Ca_2CdAs_2$, $Ca_2CdP_2$, $Eu_2CdAs_2$, $Sr_2CdAs_2$, and $Ba_2CdAs_2$**

| formula | β-$Ca_2CdAs_2$ | α-$Ca_2CdAs_2$ | $Ca_2CdP_2$ | $Eu_2CdAs_2$ | $Sr_2CdAs_2$ | $Ba_2CdAs_2$ |
|---|---|---|---|---|---|---|
| fw/g·mol$^{-1}$ | 342.40 | 342.40 | 254.50 | 566.16 | 437.48 | 536.92 |
| $T$/ °C | 23(2) | 23(2) | 23(2) | −123(2) | −123(2) | −123(2) |
| radiation, wavelength | | | λ Mo−Kα, 0.71073 Å | | | |
| space group | *Cm* (No. 8) | | | *Cmc*2$_1$ (No. 36) | | |
| $Z$ | 10 | | | 4 | | |
| unit cell dimensions | | | | | | |
| $a$/ Å | 21.5152(3) | 4.3163(5) | 4.2066(5) | 4.4418(9) | 4.4459(7) | 4.5922(5) |
| $b$/ Å | 4.3005(1) | 16.5063(19) | 16.120(2) | 16.847(4) | 16.904(3) | 17.405(2) |
| $c$/ Å | 14.3761(2) | 7.1418(8) | 7.0639(9) | 7.4985(16) | 7.5885(11) | 8.0526(8) |
| β/ deg | 110.017(1) | | | | | |
| $V$/ Å$^3$ | 1249.81(4) | 508.83(10) | 478.99(10) | 561.1(2) | 570.31(15) | 643.61(12) |
| $\rho_{calc}$/ g·cm$^{-3}$ | 4.549 | 4.470 | 3.529 | 6.702 | 5.095 | 5.541 |
| $\mu_{Mo\ K\alpha}$/ cm$^{-1}$ | 193.63 | 190.24 | 71.65 | 373.68 | 336.80 | 254.32 |
| final R indices [a] [$I > 2\sigma(I)$] | $R_1$ = 0.0461 | $R_1$ = 0.0165 | $R_1$ = 0.0152 | $R_1$ = 0.0203 | $R_1$ = 0.0238 | $R_1$ = 0.0184 |
| | $wR_2$ = 0.0747 | $wR_2$ = 0.0290 | $wR_2$ = 0.0278 | $wR_2$ = 0.0404 | $wR_2$ = 0.0404 | $wR_2$ = 0.0361 |
| final R indices [a] [all data] | $R_1$ = 0.0637 | $R_1$ = 0.0175 | $R_1$ = 0.0166 | $R_1$ = 0.0215 | $R_1$ = 0.0270 | $R_1$ = 0.0198 |
| | $wR_2$ = 0.0816 | $wR_2$ = 0.0292 | $wR_2$ = 0.0282 | $wR_2$ = 0.0407 | $wR_2$ = 0.0414 | $wR_2$ = 0.0365 |

[a] $R_1 = \Sigma||F_o| - |F_c||/\Sigma|F_o|$; $wR_2 = [\Sigma w(F_o^2 - F_c^2)^2/\Sigma w(F_o^2)^2]^{1/2}$, and $w = 1/[\sigma^2 F_o^2 + (A\cdot P)^2 + B\cdot P]$, $P = (F_o^2 + 2F_c^2)/3$; $A$ and $B$ are weight coefficients.

Details of the six data collection and structure refinement are provided in Table 1. Positional and equivalent isotropic displacement parameters, and important bond distances of α-$Ca_2CdAs_2$ and β-$Ca_2CdAs_2$ are listed in Table 2 and Table 3, respectively. Related information for the other compounds is provided in the Supporting Information (Table S1, S2). Further information in the form of CIF has been deposited with Fachinformationszentrum Karlsruhe, 76344 Eggenstein-Leopoldshafen, Germany, (fax: (49) 7247−808−666; e-mail: crysdata@fiz-karlsruhe.de) − depository CSD-number 422578 for β-$Ca_2CdAs_2$, 422579 for α-$Ca_2CdAs_2$, 422580 for $Ca_2CdP_2$, 422940 for $Sr_2CdAs_2$, 422941 for $Ba_2CdAs_2$ and 422942 for $Eu_2CdAs_2$, respectively.

**Powder X-ray Diffraction.** Powder X-ray diffraction patterns were recorded at room temperature on a Bruker AXS X-ray powder diffractometer using Cu−Kα radiation. Data were collected in a 2θ mode with a step size of 0.02°, and the counting time was 10 s. For the air-sensitive samples, the diffraction patterns were recorded at room temperature on a Rigaku Miniflex X-ray powder diffractometer, operated in a glovebox, also using Cu−Kα radiation. The collected powder patterns were used for phase identification purposes only.

**Absorption Spectrum.** The optical absorption spectra of both $Ca_2CdAs_2$ forms were measured using a U-3500 UV−vis−NIR spectrophotometer at room temperature, over the range from 1000 to 3000 nm. The measurements were done on pellets of polycrystalline samples, pressed with KBr.

**Thermal Analysis.** Thermogravimetric (TG) and Differential Scanning Calorimetry (DSC) analyses were taken on α-$Ca_2CdAs_2$ and β-$Ca_2CdAs_2$. The samples (10.2 mg for α-$Ca_2CdAs_2$ and 16.1 mg for β-$Ca_2CdAs_2$) were placed into a Mettler-Toledo TGA/DSC/1600HT instrument and run under high-purity argon gas flow for protection. Temperature was increased at a rate of 10 °C/min.

**Magnetic Susceptibility.** Field-cooled direct current magnetization measurements on a polycrystalline sample of $Eu_2CdAs_2$ (11.7 mg) were performed in a Quantum Design MPMS SQUID magnetometer. The applied magnetic field $H$ was 1000 Oe, and the temperature interval was 5−300 K. The raw data were corrected for the holder's diamagnetic contribution and converted to molar susceptibility.

**Computational Details.** To better understand the properties of the title compounds, the full potential linearized augmented plane wave method (FP-LAPW)[24] as implemented in the Wien2k code[25] was used to calculate the electronic band structures of α-$Ca_2CdAs_2$ and β-$Ca_2CdAs_2$, respectively. In this method, the unit cell is divided into nonoverlapping muffin-tin (MT) spheres and an interstitial region. The wave functions in the interstitial regions are expanded in plane waves up to $R_{MT} \times K_{max} = 7$, where $R_{MT}$ is the smallest radius of all $MT$ spheres and $K_{max}$ is the plane wave cutoff. The valence wave functions inside the $MT$ spheres are expanded up to $l_{max} = 10$ while the charge density was Fourier expanded up to $G_{max} = 12$ (au)$^{-1}$. The $MT$ radii were chosen to be 2.5 Bohr for Ca and Cd atoms, 2.3 Bohr for As atoms. The exchange correlation potential was calculated using the Perdew−Burke−Ernzerhof generalized gradient approximation (PBE-*GGA*).[26] Self-consistency was achieved using 1000 k-points in the irreducible Brillouin zone (*IBZ*). The BZ integration was performed using the tetrahedron method, and the self-consistent calculations were considered to have converged if the total energy and the charge of the system were stable within $10^{-4}$ *Ryd* and $10^{-4}$ $e^-$, respectively.

The bonding interactions and the related total and projected density of states (DOS) were calculated by using the linear muffin-tin orbital (LMTO) method[27] by the program "LMTO 4.7".[28] Exchange and correlation were treated in a local density approximation (LDA).[29] All relativistic effects except for spin−orbit coupling were taken into account by a scalar relativistic approximation.[30] Interstitial spheres had been inserted to achieve the space filling automatically.[31] The basis set included 4s, 4p, 3d for Ca, 5s, 5p, 4d for Cd, 3s, 3p, 3d for P, and 4s, 4p, 4d for As. The Ca 5p and As 4d orbitals were treated with downfolding techniques.[32] The k-space integrations were performed by the tetrahedron method,[33] and a total of 1000 k-points in the Brillouin zone were used. The Fermi level was selected as the energy reference in all calculations.

## RESULTS AND DISCUSSION

**Structure Description.** $Ca_2CdP_2$, α-$Ca_2CdAs_2$, $Eu_2CdAs_2$, $Sr_2CdAs_2$, and $Ba_2CdAs_2$ all crystallize in the orthorhombic $Yb_2CdSb_2$ structure type ($Cmc2_1$),[8a] whereas the β-$Ca_2CdAs_2$

**Table 2. Refined Atomic Coordinates and Isotropic Displacement Parameters for α-$Ca_2CdAs_2$ and β-$Ca_2CdAs_2$**

| atoms | Wyckoff | $x$ | $y$ | $z$ | $U_{eq}$ (Å$^2$)[a] |
|---|---|---|---|---|---|
| | | β-$Ca_2CdAs_2$ in $Cm$ | | | |
| Ca1 | 2a | 0.0188(2) | 0 | 0.6141(3) | 0.0140(9) |
| Ca2 | 2a | 0.1628(2) | 0 | 0.5032(3) | 0.0153(10) |
| Ca3 | 2a | 0.1897(2) | 0 | 0.7692(3) | 0.0138(9) |
| Ca4 | 2a | 0.5648(2) | 0 | 0.2134(3) | 0.0140(9) |
| Ca5 | 2a | 0.5945(2) | 0 | 0.9355(3) | 0.0152(10) |
| Ca6 | 2a | 0.7229(2) | 0 | 0.1917(3) | 0.0126(9) |
| Ca7 | 2a | 0.8264(2) | 0 | 0.5792(3) | 0.0161(10) |
| Ca8 | 2a | 0.8522(2) | 0 | 0.8524(3) | 0.0129(9) |
| Ca9 | 2a | 0.8852(2) | 0 | 0.1240(3) | 0.0156(10) |
| Ca10 | 2a | 0.8940(2) | 0 | 0.3666(3) | 0.0108(9) |
| Cd1 | 2a | 0.0000(1) | 0 | 0.0000(1) | 0.0132(4) |
| Cd2 | 2a | 0.2356(1) | 0 | 0.0322(1) | 0.0157(4) |
| Cd3 | 2a | 0.2812(1) | 0 | 0.3826(1) | 0.0133(4) |
| Cd4 | 2a | 0.4344(1) | 0 | 0.7310(1) | 0.0165(4) |
| Cd5 | 2a | 0.5269(1) | 0 | 0.4379(1) | 0.0142(4) |
| As1 | 2a | 0.0065(1) | 0 | 0.8099(2) | 0.0132(5) |
| As2 | 2a | 0.0180(1) | 0 | 0.3245(2) | 0.0122(5) |
| As3 | 2a | 0.1266(1) | 0 | 0.1058(2) | 0.0110(5) |
| As4 | 2a | 0.3040(1) | 0 | 0.7011(2) | 0.0117(5) |
| As5 | 2a | 0.3262(1) | 0 | 0.2216(1) | 0.0102(5) |
| As6 | 2a | 0.4140(1) | 0 | 0.5189(1) | 0.0104(5) |
| As7 | 2a | 0.4313(1) | 0 | 0.0201(2) | 0.0122(5) |
| As8 | 2a | 0.6186(1) | 0 | 0.6212(2) | 0.0116(5) |
| As9 | 2a | 0.7107(1) | 0 | 0.3904(2) | 0.0120(5) |
| As10 | 2a | 0.7355(1) | 0 | 0.9281(2) | 0.0132(5) |
| | | α-$Ca_2CdAs_2$ in $Cmc2_1$ | | | |
| Ca1 | 4a | 0 | 0.30024(8) | 0.5661(2) | 0.0179(3) |
| Ca2 | 4a | 0 | 0.46813(8) | 0.2290(2) | 0.0128(3) |
| Cd1 | 4a | 0 | 0.09918(3) | 0.3928(1) | 0.0136(1) |
| As1 | 4a | 0 | 0.06407(4) | 0.0165(1) | 0.0109(1) |
| As2 | 4a | 0 | 0.32003(4) | 0.0000(1) | 0.0148(2) |

[a] $U_{eq}$ is defined as one-third of the trace of the orthogonalized $U^{ij}$ tensor

**Table 3. Important Interatomic Distances (Å) in α-$Ca_2CdAs_2$ and β-$Ca_2CdAs_2$**

| atom pairs | | distances (Å) | atom pairs | | distances (Å) |
|---|---|---|---|---|---|
| | | β-$Ca_2CdAs_2$ in $Cm$ | | | |
| Cd1− | As1 | 2.783(3) | Cd2− | As3 | 2.884(3) |
| | As3 | 2.626(3) | | As5 | 2.754(2) |
| | As7 × 2 | 2.680(2) | | As10 × 2 | 2.618(2) |
| Cd3− | As5 | 2.798(2) | Cd4− | As1 × 2 | 2.667(2) |
| | As6 | 2.857(2) | | As4 | 2.689(2) |
| | As9 × 2 | 2.656(2) | | As6 | 2.929(3) |
| Cd5− | As2 × 2 | 2.665(2) | | | |
| | As6 | 3.033(3) | | | |
| | As8 | 2.697(3) | | | |
| Ca1− | As1 | 2.917(5) | Ca2− | As2 | 3.290(5) |
| | As2 | 4.157(5) | | As4 | 3.378(5) |
| | As6 × 2 | 3.077(3) | | As8 × 2 | 3.083(3) |
| | As8 × 2 | 3.016(3) | | As9 × 2 | 3.076(3) |
| Ca3− | As1 | 4.177(4) | Ca4− | As2 × 2 | 3.049(3) |
| | As4 | 2.943(5) | | As3 × 2 | 3.192(3) |
| | As8 × 2 | 3.043(3) | | As7 | 3.242(5) |
| | As10 × 2 | 3.045(3) | | As9 | 3.296(5) |
| Ca5− | As1 × 2 | 3.022(3) | Ca6− | As3 × 2 | 2.948(3) |
| | As3 × 2 | 3.152(4) | | As5 × 2 | 3.017(3) |
| | As7 | 4.090(5) | | As9 | 2.956(5) |
| | As10 | 3.070(5) | | As10 | 3.890(5) |
| Ca7− | As1 | 4.150(5) | Ca8− | As1 | 3.574(4) |
| | As4 × 2 | 2.916(3) | | As4 × 2 | 2.981(3) |
| | As6 × 2 | 3.169(3) | | As7 × 2 | 3.244(3) |
| | As9 | 2.989(5) | | As10 | 3.062(5) |
| Ca9− | As2 | 3.292(5) | Ca10− | As2 | 2.930(5) |
| | As5 × 2 | 3.069(3) | | As5 × 2 | 3.002(3) |
| | As7 × 2 | 2.976(3) | | As6 × 2 | 2.993(3) |
| | As10 | 3.478(5) | | As9 | 4.073(4) |
| | | α-$Ca_2CdAs_2$ in $Cmc2_1$ | | | |
| Cd1− | As1 | 2.7497(9) | | | |
| | As1 | 2.8357(8) | | | |
| | As2 × 2 | 2.6499(5) | | | |
| Ca1− | As1 × 2 | 3.1304(11) | Ca2− | As1 × 2 | 3.0256(10) |
| | As2 × 2 | 2.9701(10) | | As1 × 2 | 3.0773(10) |
| | As2 | 3.1161(16) | | As2 | 2.9413(15) |
| | As2 | 4.0561(17) | | As2 | 3.9965(15) |

crystallizes in a new, closely related monoclinic structure with the space group $Cm$. Since the structure of $Yb_2CdSb_2$ and its relationship to other well-known types have been well discussed previously,[8a] in this paper the structural description will be mainly focused on β-$Ca_2CdAs_2$ and the existing polymorphism.

A schematic structural comparison between α-$Ca_2CdAs_2$ and β-$Ca_2CdAs_2$ is presented in Figures 1 and 2. As seen from Figure 1, both are layered structures, based of corner-shared $CdAs_4$ tetrahedra. Topologically similar polyanionic fragments of corner-shared tetrahedra have also been observed in $A_9Cd_{4+x}Pn_9$ ($A$ = Ca, Sr, Yb, Eu; $Pn$ = Sb, Bi).[7d] In β-$Ca_2CdAs_2$, the $CdAs_4$ tetrahedra are distorted with Cd−As bonds ranging from 2.618(2) Å to 3.033(3) Å (Table 3). These distances are comparable to the Cd−As contacts in other arsenides, such as $Ba_2Cd_2As_3$,[13] $SrCd_2As_2$,[34] $BaCd_2As_2$,[35] and so forth, and indicate covalent interactions between Cd and As atoms, also supported by the theoretical calculations (vide infra). We note that there are 5 crystallographically independent Cd atoms, and the tetrahedra centered by Cd1, Cd2, and Cd3 have very similar bonding distances between 2.618(2) and 2.884(3) Å, that is, are less distorted compared to the Cd4- and Cd5-centered ones, where the deviations from the ideal tetrahedral geometry are most significant. From the corresponding bond angles, one can see that the angles involving Cd5 for example, vary from 92.25(7)° to 118.24(6)°. Understandably this is the place in the structure where three $CdAs_4$ share a corner. For comparison, α-$Ca_2CdAs_2$ does not have such a feature, and the $CdAs_4$ tetrahedra are closer to the regular shape with Cd−As bonds falling into a much narrower range—from 2.6499(5) to 2.8357(8) Å—and the corresponding angles varying from about 96° to about 110°.

The structural similarity between α-$Ca_2CdAs_2$ and β-$Ca_2CdAs_2$ can be clearly seen from Figure 2, where only cut-outs from the $[CdAs_2]^{4-}$ layers are depicted. It is evident that the repeating unit in α-$Ca_2CdAs_2$ (shown in blue) is also present in the β-form,


dx.doi.org/10.1021/ic200286t |Inorg. Chem. 2011, 50, 8020–8027

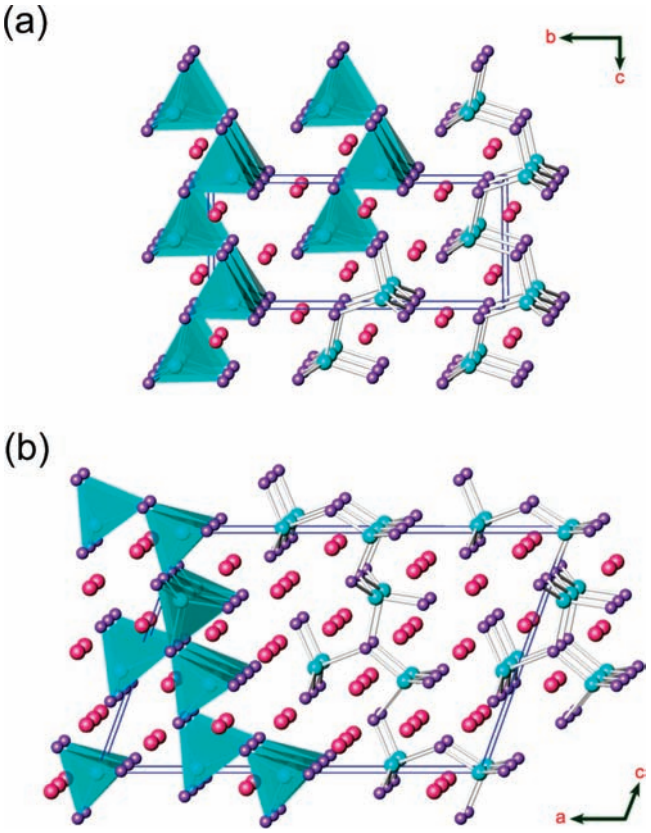


**Figure 1.** Combined polyhedral and ball-and-stick representations of the structures for α-$Ca_2CdAs_2$ (a) and β-$Ca_2CdAs_2$ (b). The Cd atoms at the centers of As tetrahedra (translucent) are shown as light blue spheres, and the As atoms as apexes are drawn as purple spheres. The Ca cations are indicated as red spheres. The orthorhombic α-$Ca_2CdAs_2$ structure is projected down the *a*-axis, and the monoclinic β-$Ca_2CdAs_2$ structure is projected down the *b*-axis, respectively. Unit cells are outlined.

where an additional $CdAs_4$ tetrahedron (along the *a*-axis) is "inserted". Another comparison of the topology of the repeating units (shown in different projections) of these two structures is given in Supporting Information, Figure S1.

The coordination environments of the cations in both compounds are worthy of a brief mention too. The coordination spheres for the cations in α-$Ca_2CdAs_2$ and β-$Ca_2CdAs_2$ are provided in Supporting Information, Figure S2. For a relatively small cation such as $Ca^{2+}$, an octahedral coordination is very common and could be expected. Indeed, in the orthorhombic compounds $A_2CdSb_2$, one of the cation sites (*A*2) is in a distorted octahedral environment, while the other $A^{2+}$ cation (*A*1) is found, if only the next nearest Sb atoms were considered, in a polyhedron resembling a square pyramid (CN 5).[8a]

For α-$Ca_2CdAs_2$, both independent Ca atoms are in square pyramidal environments, which is somewhat surprising given its isotypism with the antimonides (vide infra). Ca1, for example, has five As atoms with Ca1—As distances ranging from 2.9701(10) Å to 3.1161(16) Å. The "open" square face is capped by another, very distant As (As2), which is 4.0561(17) Å away from Ca1. For comparison, the corresponding Ca1—Sb3 and Yb1—Sb2 distances in $Ca_2CdSb_2$ and $Yb_2CdSb_2$ are 3.741(2) Å and 3.739(2) Å, respectively.[8a] This indicates that there are subtle differences between the arsenides and the antimonides of this family, and this conundrum has received additional consideration in the theoretical section.

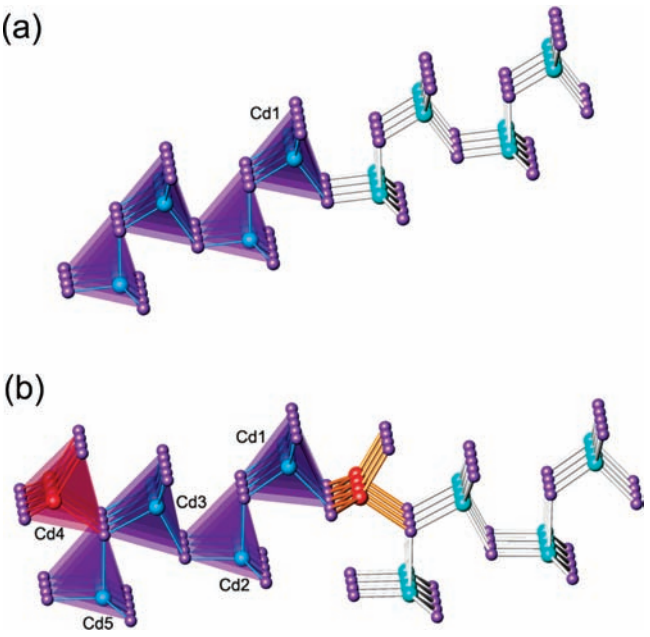


**Figure 2.** Structural relationship between the α-$Ca_2CdAs_2$ (a) and β-$Ca_2CdAs_2$ (b) structures, exemplified by selected fragments of their $^2_\infty[CdAs_2]^{4-}$ polyanionic layers. The structural difference in the repeating sequence is highlighted is red. See text for details.

For β-$Ca_2CdAs_2$, Ca2, Ca4, Ca8, and Ca9 are in distorted octahedral environments of As atoms, where the longest Ca—As separation is 3.574(4) Å. Atomic distances in this range indicate reasonable bonding interactions, based on the Pauling metallic radii of Ca and As. The rest of the Ca cations' coordination polyhedra are square pyramids of As atoms, with Ca—As contacts on the order of 3.0—3.2 Å (Table 3), similar to the average Ca1—As distances in α-$Ca_2CdAs_2$ (above). The "missing" sixth As atoms to complete the octahedra are about 4 Å away.

**Thermal Stability.** The possibility for a phase transition related to α-$Ca_2CdAs_2$ and β-$Ca_2CdAs_2$ was studied through TG-DSC measurements. These two Ca-compounds appear to irreversibly decompose above 750 °C with significant weight losses taking place (see Supporting Information), respectively. The onset of decomposition of β-$Ca_2CdAs_2$ is around 700 °C, while α-$Ca_2CdAs_2$ seems to begin decomposing at temperatures just above 500 °C. This observation is supported by annealing crystals of both polymorphs in sealed tubes—they retained (after a week) their structure and integrity when treated below the respective decomposition temperatures deduced from the DSC data, and transformed into simple binary phases above those temperatures.

**Optical Absorption Spectra.** The optical absorption spectra were measured on the polycrystalline powder samples of both α-$Ca_2CdAs_2$ and β-$Ca_2CdAs_2$, and the results are provided in Supporting Information, Figure S3. For β-$Ca_2CdAs_2$, the onset of an absorption edge starting from 1305 nm is clearly seen, corresponding to a small band gap of about 0.95 eV and is consistent with its black color. The absorption spectrum of α-$Ca_2CdAs_2$ shows that the intensity changes gradually with the wavelength, making it difficult to identify the corresponding band gap. An unrecognized impurity phase or traces of flux metal in the sample


dx.doi.org/10.1021/ic200286t |*Inorg. Chem.* 2011, 50, 8020–8027

might account for this ambiguity. Ongoing efforts to grow large single crystals of this compound, suitable for the property measurements may provide a remedy for this problem.

**Magnetic Susceptibility.** A plot of the magnetic susceptibility versus temperature of polycrystalline $Eu_2CdAs_2$ is shown in Figure 3. Above 25 K, the sample exhibits paramagnetic behavior with inverse molar susceptibility that can be fitted to a line, that is, to the Curie–Weiss law $\chi(T) = C/(T - \theta)$, where $\chi$ is the molar susceptibility, $C$ is the Curie constant $(C = N_A\mu_{eff}^2/k_B)$ and $\theta$ is the Weiss temperature. A fit of the data ($T > 30$ K), as shown in the inset yields an effective moment of 7.75 $\mu_B$ per Eu atom, indicating that all Eu cations are divalent. This result is not unexpected, given that all other isotypic compounds form with the alkaline-earth metal cations or $Yb^{2+}$.[8] The intercept of the linear fit also suggest possible ferromagnetic coupling of the spins of Eu 4f electrons at very low temperature, as inferred from the positive Weiss temperature $\theta$ = 9 K. Ferromagnetic ordering has been observed in other Eu-containing Zintl phases such as $EuGa_2P_2$ and $EuGa_2As_2$.[36]

**Electronic Structure.** To better understand the structure and bonding, as well as the observed relatively wide band gap semiconducting properties, first principles calculations were performed on the structures of α-$Ca_2CdAs_2$ and β-$Ca_2CdAs_2$. The computed band structures are shown in Figure 4. As expected from the optical measurements discussed above, both compounds are direct gap semiconductors with separation between the top of the valence band and the bottom of the conduction band of about 0.9 eV for α-$Ca_2CdAs_2$ and about 0.7 eV for β-$Ca_2CdAs_2$, respectively. The small difference between the computed band-gaps can be correlated with the difference in the states around the Fermi level—they are predominantly contributed by the d-orbitals from the Ca cations and p-orbitals from As anions, as shown in Figure 5 and Figure 6. As we analyze below, the cation–anion interactions in both compounds are not the same, and the Ca–As bonds in β-$Ca_2CdAs_2$ (the structure with more distorted Ca polyhedra) can be expected to be slightly less ionic. Consequently, a smaller energy separation between the corresponding bonding and antibonding states and a narrower band gap results in the β-polymorph. Preliminary resistivity measurements on single-crystals of $Eu_2CdAs_2$ also corroborate the intrinsic semiconducting properties, with about 0.3 eV

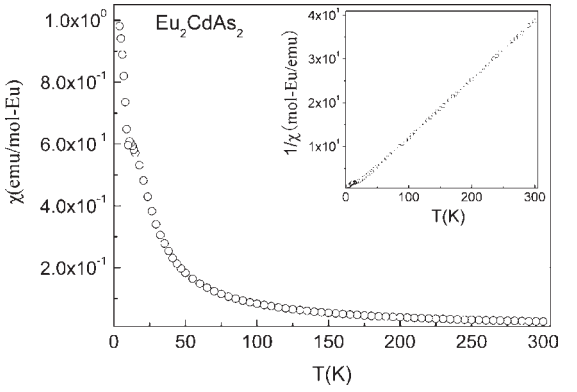


**Figure 3.** Temperature-dependent magnetic susceptibility of $Eu_2CdAs_2$. The measurements were carried out upon cooling from 300 down to 4 K at a field of 1000 Oe. Inset: Inverse susceptibility as a function of the temperature and a linear fit to the Curie–Weiss law.

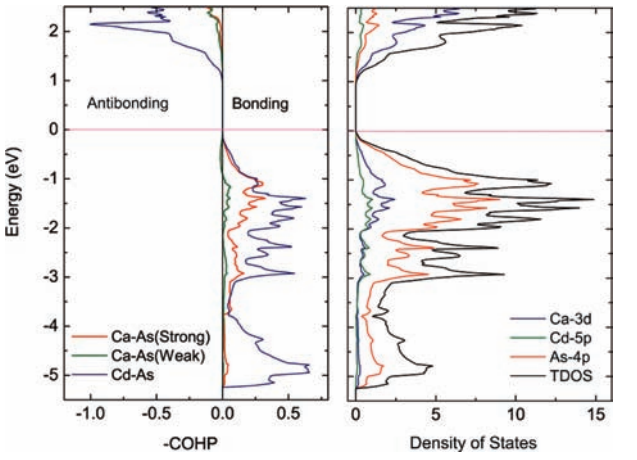


**Figure 5.** Calculated COHP of various interatomic interactions for α-$Ca_2CdAs_2$ (Left). The total DOS and the projected DOS are plotted on the same energy scale (Right).

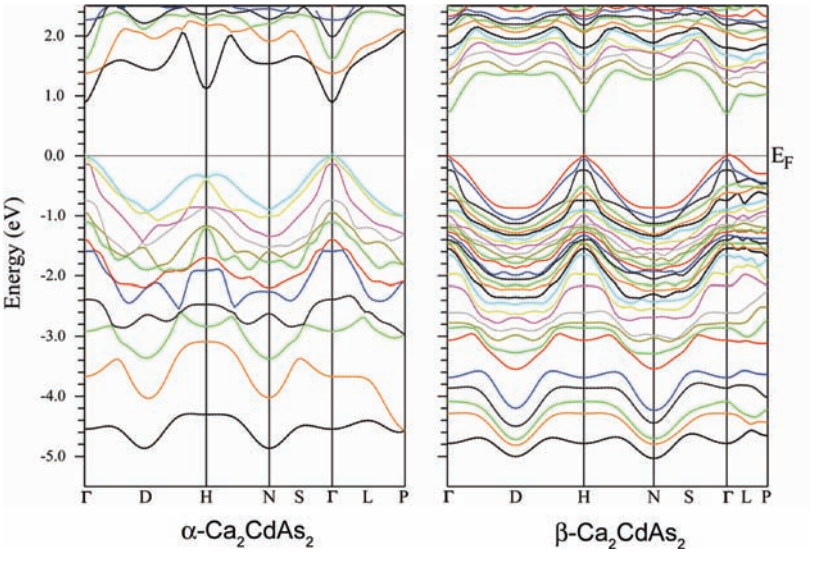


**Figure 4.** Calculated electronic band structures for α-$Ca_2CdAs_2$ and β-$Ca_2CdAs_2$, respectively. The Fermi level is chosen as the energy reference at 0 eV.


dx.doi.org/10.1021/ic200286t |Inorg. Chem. 2011, 50, 8020–8027

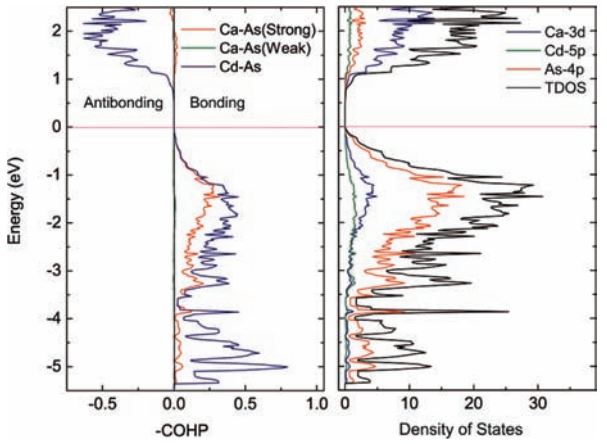


**Figure 6.** Calculated COHP of various interatomic interactions for $\beta$-$Ca_2CdAs_2$ (Left). The total DOS and the projected DOS are plotted on the same energy scale (Right) and the Fermi level is selected as the energy reference.

Arrhenius-like activation energy deduced from ln $\rho(T)$ (Supporting Information). Similar conclusion was drawn from the calculations on the previously reported antimonides,[8] which have much smaller band-gaps (ca. 0.1 eV).[8a] We note here that the theoretical results underestimate the band gap, compared with the experiment, which is acceptable within the LDA/GGA level of theory.

As we mentioned above, the coordination environments of the Ca cations in α-$Ca_2CdAs_2$ differ slightly from those of $A_2CdSb_2$. Therefore, we classified the Ca−As interactions as "strong" and "weak" ones according to their distances. The distances of 3.6 Å and shorter were considered "strong" and the long about 4 Å contacts, listed in Table 3, were dubbed "weak". Then, the Ca−As interactions were examined by means of their crystal orbital Hamilton population (COHP), as shown in Figure 5. The calculated average COHP indicates that the Cd−As bonding is the strongest, exhibiting two prominent peaks at around −2 and −5 eV. The COHP of the "strong" Ca−As bonds has several broad bands appearing right below the Fermi level, confirming the importance of the Ca−As bonding to the overall structure. The COHP curves for the "weak" Ca−As interactions are different between α-$Ca_2CdAs_2$ and $\beta$-$Ca_2CdAs_2$. For α-$Ca_2CdAs_2$, weak, but *not* negligible bonding interactions can still be observed (Figure 5). However, for the latter, the calculations indicate the long Ca−As pairs (≈ 4 Å) are almost nonbonding (Figure 6).

Another aspect worthy of specific mention is the COHP curves just above the Fermi level. For α-$Ca_2CdAs_2$, the COHP curves for the "strong" Ca−As show a small region of antibonding character, while the same energy window becomes bonding in $\beta$-$Ca_2CdAs_2$. The results above indicate that although α-$Ca_2CdAs_2$ and $\beta$-$Ca_2CdAs_2$ have the similar layered structures and analogous cation environments, the corresponding Ca−As interactions are subtly different. Such differences could help explain the wider band gap of α-$Ca_2CdAs_2$ compared to that of $\beta$-$Ca_2CdAs_2$.

## CONCLUSIONS

In conclusion, the new Zintl compounds $Ca_2CdP_2$, $Ca_2CdAs_2$, $Sr_2CdAs_2$, $Ba_2CdAs_2$, and $Eu_2CdAs_2$ have been synthesized, and their structures have been established via X-ray single-crystal diffraction. The arsenides are semiconductors with small direct band gaps, which are supported by the optical absorption spectra as well as the density functional calculations. The distorted coordination environments of the cations in combination with the noncentrosymmetric space groups of these compounds also suggest that they could be suitable materials for nonlinear optic applications in the near-IR region. The Compound $Eu_2CdAs_2$, which appears to be an intrinsic small band gap semiconductor, could also be of interest as a potential thermoelectric material.

## ASSOCIATED CONTENT

**Supporting Information.** The X-ray crystallographic files in CIF format were provided for all title compounds; the refined atomic coordinates for $Ca_2CdP_2$, $Eu_2CdAs_2$, $Sr_2CdAs_2$, and $Ba_2CdAs_2$; refined interatomic distances in $Ca_2CdP_2$, $Eu_2CdAs_2$, $Sr_2CdAs_2$, and $Ba_2CdAs_2$; drawings of the cations' coordination environments for compounds and the $^2_\infty[CdAs_2]^{4-}$ polyanionic layers of α-$Ca_2CdAs_2$ and $\beta$-$Ca_2CdAs_2$, viewed down in a direction normal to the layers; the absorption spectrum of sample α-$Ca_2CdAs_2$; TG-DSC measurements of α-$Ca_2CdAs_2$ and $\beta$-$Ca_2CdAs_2$; a representative powder diffraction pattern of $Eu_2CdAs_2$; four-probe resistivity measurements on single-crystals of $Eu_2CdAs_2$. This material is available free of charge via the Internet at http://pubs.acs.org.

## AUTHOR INFORMATION

### Corresponding Author

*Phone: (531) 883-62519 (S.-Q.X.), (302) 831-8720 (S.B.). Fax: (531) 883-64864 (S.-Q.X.), (302) 831-6335 (S.B.). E-mail: shqxia@sdu.edu.cn (S.-Q.X.), bobev@udel.edu (S.B.).

## ACKNOWLEDGMENT

S.-Q.X. acknowledges financial support of the start-up grants from the Shandong University, the State Key Laboratory of Crystal Materials and the Scientific Research Foundation for the Returned Overseas Chinese Scholars, State Education Ministry. S.B. acknowledges the U.S. Department of Energy through a grant (DE-SC0001360) for partial financial support. This work is also sponsored by the National Natural Science Foundation of China (Grant 20901047, 51021062, 50990061), the Shandong Provincial Natural Science Foundation (Grant ZR2010BM003), and the 973 Program of the People's Republic of China (Grant 2010CB630702). H.H. thanks the International Centre for Diffraction Data (ICDD) for the 2011 Ludo Frevel Fellowship

## REFERENCES

(1) *Chemistry, Structure and Bonding of Zintl Phases and Ions*; Kauzlarich, S. M., Ed.; VCH: Weinheim, Germany, 1996 and references therein.

(2) Nesper, R. *Angew. Chem., Int. Ed. Engl.* **1991**, *30*, 789.

(3) (a) Zintl, E. *Angew. Chem.* **1939**, *52*, 1. (b) Laves, F. *Naturwissenschaften* **1941**, *29*, 244.

(4) (a) Klem, M. T.; Vaughey, J. T.; Harp, J. G.; Corbett, J. D. *Inorg. Chem.* **2001**, *40*, 7020. (b) Mudring, A. V.; Corbett, J. D. *Inorg. Chem.* **2005**, *44*, 5636.

(5) Lam, R.; Zhang, J. J.; Mar, A. J. *Solid State Chem.* **2000**, *150*, 371.

(6) (a) Chan, J. Y.; Olmstead, M. M.; Kauzlarich, S. M.; Webb, D. J. *Chem. Mater.* **1998**, *10*, 3583. (b) Kim, H.; Condron, C. L.; Holm, A. P.; Kauzlarich, S. M. *J. Am. Chem. Soc.* **2000**, *122*, 10720. (c) Holm, A. P.;

Olmstead, M. M.; Kauzlarich, S. M. *Inorg. Chem.* **2003**, *42*, 1973. (d) Holm, A. P.; Park, S.-M.; Condron, C. L.; Kim, H.; Klavins, P.; Grandjean, F.; Hermann, R. P.; Long, G. J.; Kanatzidis, M. G.; Kauzlarich, S. M.; Kim, S.-J. *Inorg. Chem.* **2003**, *42*, 4660. (e) Brown, D. E.; Johnson, C. E.; Grandjean, F.; Hermann, R. P.; Kauzlarich, S. M.; Holm, A. P.; Long, G. J. *Inorg. Chem.* **2004**, *43*, 1229. (f) Park, S. M.; Kim, S. J.; Kanatzidis, M. G. *Inorg. Chem.* **2005**, *44*, 4979.

(7) (a) Bobev, S.; Thompson, J. D.; Sarrao, J. L.; Olmstead, M. M.; Hope, H.; Kauzlarich, S. M. *Inorg. Chem.* **2004**, *43*, 5044. (b) Bobev, S.; Merz, J.; Lima, A.; Fritsch, V.; Thompson, J. D.; Sarrao, J. L.; Gillessen, M.; Dronskowski, R. *Inorg. Chem.* **2006**, *45*, 4047. (c) Xia, S.-Q.; Bobev, S. *Inorg. Chem.* **2007**, *46*, 874. (d) Xia, S.-Q.; Bobev, S. *J. Am. Chem. Soc.* **2007**, *129*, 10011. (e) Xia, S.-Q.; Bobev, S. *Inorg. Chem.* **2008**, *47*, 1919. (f) Saparov, B.; Bobev, S. *Inorg. Chem.* **2010**, *49*, 5173. (g) Xia, S.-Q.; Bobev, S. *Chem. Mater.* **2010**, *22*, 840.

(8) (a) Xia, S.-Q.; Bobev, S. *J. Am. Chem. Soc.* **2007**, *129*, 4049. (b) Saparov, B.; Saito, M.; Bobev, S. *J. Solid State. Chem.* **2011**, *184*, 432.

(9) (a) Chan, J. Y.; Kauzlarich, S. M.; Klavins, P.; Shelton, R. N.; Webb, D. J. *Chem. Mater.* **1997**, *9*, 3132. (b) Jiang, J.; Kauzlarich, S. M. *Chem. Mater.* **2006**, *18*, 435.

(10) (a) Sánchez-Portal, D.; Martin, R. M.; Kauzlarich, S. M.; Pickett, W. E. *Phys. Rev. B* **2002**, *65*, 144414. (b) Holm, A. P.; Kauzlarich, S. M.; Morton, S. A.; Waddill, G. D.; Pickett, W. E.; Tobin, J. G. *J. Am. Chem. Soc.* **2002**, *124*, 9894.

(11) Fisher, I. R.; Bud'ko, S. L.; Song, C.; Canfield, P. C.; Ozawa, T. C.; Kauzlarich, S. M. *Phys. Rev. Lett.* **2000**, *85*, 1120.

(12) (a) Brown, S. R.; Kauzlarich, S. M.; Gascoin, F.; Snyder, G. J. *Chem. Mater.* **2006**, *18*, 1873. (b) Kauzlarich, S. M.; Brown, S. R.; Snyder, G. J. *Dalton Trans.* **2007**, *21*, 2099.

(13) Saparov, B.; He, H.; Zhang, X. H.; Greene, R.; Bobev, S. *Dalton Trans.* **2010**, *39*, 1063.

(14) Dmitriev, V. G.; Gurzadyan, G. G.; Nikogosyan, D. N. *Handbook of Nonlinear Optical Crystals*, 3rd ed.; Springer: Berlin, Germany, 1999.

(15) Boyd, G. D.; Buehler, E.; Storz, F. G. *Appl. Phys. Lett.* **1971**, *18*, 301.

(16) Boyd, G. D.; Kasper, H.; Mcfee, J. H. *IEEE J. Quantum Electron.* **1971**, *QE 7*, 563.

(17) Isaenko, L.; Yelisseyev, A.; Lobanov, S.; Petrov, V.; Rotermund, F.; Zondy, J. J.; Knippels, G. H. M. *Mater. Sci. Semicond. Process.* **2001**, *4*, 665.

(18) Ren, P.; Qin, J. G.; Chen, C. T. *Inorg. Chem.* **2003**, *42*, 8.

(19) Phanon, D.; Gautier-Luneau, I. *Angew. Chem., Int. Ed.* **2007**, *46*, 8488.

(20) (a) Kim, Y.; Seo, I. S.; Martin, S. W.; Baek, J.; Halasyamani, P. S.; Arumugam, N.; Steinfink, H. *Chem. Mater.* **2008**, *20*, 6048. (b) Chung, I.; Malliakas, C. D.; Jang, J. I.; Canlas, C. G.; Weliky, D. P.; Kanatzidis, M. G. *J. Am. Chem. Soc.* **2007**, *129*, 14996. (c) Bera, T. K.; Jang, J. I.; Ketterson, J. B.; Kanatzidis, M. G. *J. Am. Chem. Soc.* **2009**, *131*, 75.

(21) *Bruker APEX2*; Bruker AXS Inc.: Madison, WI, 2005.

(22) Sheldrick, G. M. *SHELXTL*; University of Göttingen, Göttingen, Germany, 2001.

(23) (a) Parthé, E.; Gelato, L. M. *Acta Crystallogr.* **1984**, *A40*, 169. (b) Gelato, L. M.; Parthé, E. *J. Appl. Crystallogr.* **1987**, *20*, 139.

(24) (a) Madsen, G. K. H.; Blaha, P.; Schwarz, K.; Sjöstedt, E.; Nordström, L. *Phys. Rev. B* **2001**, *64*, 195134. (b) Schwarz, K.; Blaha, P.; Madsen, G. K. H. *Comput. Phys. Commun.* **2002**, *147*, 71.

(25) Blaha, P.; Schwarz, K.; Madsen, G. K. H.; Kvasnicka, D.; Luitz, J. *WIEN2k, An Augmented Plane Wave + Local Orbitals Program for Calculating Crystal Properties*; Technische Universität Wien: Vienna, Austria, 2001.

(26) Perdew, J. P.; Burke, S.; Ernzerhof, M. *Phys. Rev. Lett.* **1996**, *77*, 3865.

(27) (a) Andersen, O. K. *Phys. Rev. B* **1975**, *12*, 3060. (b) Andersen, O. K.; Jepsen, O. *Phys. Rev. Lett.* **1984**, *53*, 2571. (c) Andersen, O. K.; Jepsen, O.; Glötzel, D. In *Highlights of condensed matter theory*; Bassani, F., Fumi, F., Tosi, M. P., Eds.; NorthHolland: New York, 1985; (d) Andersen, O. K. *Phys. Rev. B* **1986**, *34*, 2439. (e) Skriver, H. L. *The LMTO Method*; Springer: Berlin, Germany, 1984.

(28) Jepsen, O.; Andersen, O. K. *The Stuttgart TB-LMTO Program*, Version 4.7; Max-Planck-Institut für Festkörperforschung: Stuttgart, Germany.

(29) Von Barth, U.; Hedin, L. *J. Phys. C* **1972**, *5*, 1629.

(30) Koelling, D. D.; Harmon, B. N. *J. Phys. C* **1977**, *10*, 3107.

(31) Jepsen, O.; Andersen, O. K. *Z. Phys. B* **1995**, *97*, 35.

(32) Lambrecht, W. R. L.; Andersen, O. K. *Phys. Rev. B* **1986**, *34*, 2439.

(33) Blöchl, P. E.; Jepsen, O.; Andersen, O. K. *Phys. Rev. B.* **1994**, *49*, 16223.

(34) Mewis, A. *Z. Naturforsch.* **1980**, *35B*, 939.

(35) Kluefers, P.; Mewis, A. *Z. Kristallogr.* **1984**, *169*, 135.

(36) Goforth, A. M.; Hope, H.; Condron, C. L.; Kauzlarich, S. M.; Jensen, N.; Klavins, P.; MaQuilon, S.; Fisk, Z. *Chem. Mater.* **2009**, *21*, 4480.